https://doi.org/10.5194/egusphere-2026-2738
Preprint. Discussion started: 4 June 2026

Atmospheric Concentration of Black Carbon over Africa: Hotspot Regions, Seasonal Dynamics and Future Projections from Bias-Adjusted AerChemMIP Models

Matthews Nyasulu[1], Yan-Lin Zhang[1, 2]*, Cao Fang[1,2], Md. Mozammel Haque[1,2]

[1]School of Ecology and Applied Meteorology, Nanjing University of Information Science and Technology, Nanjing,210044, China.
[2]Atmospheric Environment Center, Joint Laboratory for International Cooperation on Climate and Environmental Change, Ministry of Education, Nanjing University of Information Science and Technology, Nanjing, 210044, China

Corresponding author: Yan-Lin Zhang (dryanlinzhang@outlook.com, zhangyanlin@nuist.edu.cn).

Abstract. Black carbon (BC) is one of the most potent short-lived climate forcers, accelerating global warming and posing risks to human health. Despite its climatic and health implications, BC remains poorly characterized across much of Africa. Here, we use bias-adjusted Aerosol Chemistry Model Intercomparison Project (AerChemMIP) simulations to identify hotspot regions, analyse long-term trends and assess key drivers of its spatial-temporal changes. Although models reproduce the spatial patterns of BC, they systematically underestimate concentration over Central Africa. The bias-adjusted simulations indicate that BC concentration is highest in Central Africa, where annual mean values exceed 1.5 μg m^{-3} and seasonal peaks reach approximately 3 μg m^{-3}, while North Africa and Madagascar exhibit much lower concentration (0.1 μg m^{-3}). Seasonal dynamics is dominated by dry-season enhancements driven by biomass burning while lower concentration is detected during the wet season due to reduced burning activities and enhanced wet deposition. In addition, long-range transport of BC from Europe enhances concentration in North Africa. The Sen's slope and Mann-Kendall trend test revealed significant BC increase in regions with rapid economic development such as southern Nigeria, central Ethiopia, Rwanda and northern Egypt. Future projections under SSP370SST show continued BC increase (~0.5–1.0% yr^{-1}) in North, West and East Africa until mid-century while a significant decrease in parts of Central and Southern Africa until late-century. These findings highlight the need for targeted control strategies and stronger regulatory policies to reduce BC concentration in hotspot regions while sustaining and reinforcing mitigation efforts in regions with declining trends.

Key words: Black carbon, AerChemMIP, Biomass burning, Mitigation strategies, Africa

1. Introduction

BC is a major light-absorbing aerosol that contributes substantially to atmospheric warming through its strong absorption of solar radiation (Boucher and Haywood, 2001; Samset et al., 2014). BC heats the atmosphere via positive radiative forcing and can influence atmospheric circulation and precipitation patterns (Jacobson, 2001; Meehl et al., 2008). When deposited on snow and ice, it reduces surface albedo and accelerates melting through the snow-albedo feedback (Ramanathan and Carmichael, 2008; Bond et al., 2013). In addition to its climatic effects, numerous epidemiological studies have linked short and long-term BC exposure to cardiovascular and respiratory diseases (Janssen et al., 2011; Segersson et al., 2017; Ghosh et al., 2021). BC also carries toxic compounds such as polycyclic aromatic hydrocarbons (PAHs), further increasing health risks (Ali et al., 2021). Although the atmospheric lifetime of

https://doi.org/10.5194/egusphere-2026-2738
Preprint. Discussion started: 4 June 2026

BC is relatively short (days to weeks), it can be extended in dry regions with weak winds and limited precipitation (Cape et al, 2012).

BC is emitted primarily from incomplete combustion of fossil fuels, biofuels and biomass burning, including forest fires and agricultural waste burning (Bond et al., 2013; Hsu et al., 2013). Sub-Saharan Africa (SSA) is one of the global hotspots of BC emissions, with seasonal biomass burning representing the dominant source (Giwa et al., 2014; Kirago et al., 2022; Kirchstetter et al., 2003). Despite Africa's importance in the global BC budget, large uncertainties on concentration levels, sources and its associated climatic and health implications remain high due to scarce long-term ground-based observations, limited monitoring capacity and high costs of regulatory instruments (Anand et al., 2024). Existing studies are mostly based on short-term campaigns or limited regional analyses, restricting the ability to assess continent-wide trends or quantify climate and health impacts (Alli et al., 2021; Chiloane et al., 2017; Dawoud et al., 2023; Doumbia et al., 2012). Atmospheric models therefore play a key role in improving the understanding of BC distribution, trends, sources and quantify their health and climatic implications. The AerChemMIP, part of Coupled Model Intercomparison Project phase 6 (CMIP 6) (Collins et al., 2017), provides a coordinated framework for evaluating near-term climate forcers, reactive gases, aerosols and their precursors. AerChemMIP models can simulate BC over the historical period (1850-2014) and future scenarios (2015-2100) under different Shared Socioeconomic Pathways (SSPs), allowing investigation of historical aerosol-climate interactions, attribution of past changes in BC and assessment of future evolution under different emission pathways and mitigation scenarios. AerChemMIP simulations have been widely used to analyse aerosol distributions, composition, climatic and health impacts (Allen et al., 2020; Thornhill et al., 2021; Toolan et al., 2025; Turnock et al., 2020).

Despite the critical role of BC in climate forcing and air quality, its spatial distribution, temporal evolution and underlying drivers remain understudied in many parts of Africa, largely due to the scarcity of comprehensive, continent-wide observational and modeling studies. This persistent knowledge gap undermines Africa's effective development, region-specific mitigation strategies as pollution emissions are increasing and insufficiently quantified (Keita et al., 2021). Here, we address this limitation by systematically investigating the spatial hotspots, seasonal variability and long-term trends of near surface BC across Africa using bias-adjusted AerChemMIP simulations in combination with Modern-Era Retrospective analysis for Research and Applications, Version 2 (MERRA-2) reanalysis datasets. In addition, the study assesses its projected future evolution, thereby providing a robust scientific basis for targeted emission control policies.

2. **Data and Methods**

2.1. The AerChemMIP

The AerChemMIP is one of the recently included MIPs in the CMIP-6, designed to quantify the climatic and air quality impact of aerosols and chemically reactive gases in the atmosphere (Collins et al., 2017; Griffiths et al., 2025). It includes short-lived climate forcers (SLCFs) such as methane, ozone, aerosols and their precursors such as nitrous oxide and ozone-depleting halocarbons. AerChemMIP simulates both historical and future pollutant scenarios, following the guidelines detailed in Collins et al. (2017). In terms of historical simulation, aerosols and ozone span

https://doi.org/10.5194/egusphere-2026-2738
Preprint. Discussion started: 4 June 2026

from 1850 to 2014, while those with halocarbons span from 1950 to 2014. Historical simulations are run under two configurations: Prescribed sea surface temperature (histSST), which isolates the direct atmospheric feedback to specific pollutants by keeping the ocean state constant. They also simulate BC with fully coupled atmosphere-ocean general circulation (hist), designed to capture integrated climate feedback by incorporating full climate system response, including oceans and other components (Collins et al., 2017). Future simulations use SSPs with focus on regional rivalry, where pollution control is weak and targets radiative force of 7.0 W m^2 by the year 2100 (SSP370). Under SSP370, economic development is slow, reliability on fossil fuel is high, slow technological development and high challenge to mitigation. Furthermore, there is low progress on human development and income growth, while lack of effective institutions, which results into increased challenges to adaptation (O'Neill et al., 2017). In this study, we utilized histSST and SSP370SST to facilitate a more direct understanding of how regional emissions such as those from biomass burning, fossil fuel and traffic interact with atmospheric transport and removal processes to shape BC distribution and trends, with reduced influence from ocean-atmosphere feedbacks over Africa. Five models were selected for analysis, which had data accessible during the time of analysis (Table 1). Although AeroChemMIP models follow common CMIP6 forcing protocols and emission inventories (Hoesly et al., 2018), differences in aerosol parameterizations, transport processes, deposition schemes and model physics can lead to substantial inter-model variability in simulated BC. The historical analyses in this study covers the period of 1981-2014 while future projections cover the period of 2015-2100. Three future time slices were considered: 2015-2040 (near future), 2041-2070 (mid-century) and 2071-2100 (late century). The study domain covers the entire African continent, as shown in Fig.S1 and has been further partitioned into sub-regions; North Africa, West Africa, Central Africa, East Africa, Southern Africa and the Madagascar Island for targeted regional analysis.

Table 1. Summary of the AerChem-CMIP6 models used for the analysis

Model	Initial grid size (lon × lat)	Chemistry scheme	Aerosol treatment	Key reference
GISS-E2-1G	2.5º × 2º	GISS Chemistry	Prescribed	Kelley et al. (2020)
MIROC6-LE	1.4º × 1.4º	CHASER	SPRINTARS aerosol model	Shiogama et al. (2023)
MRI-ESM2-0	1º × 1º	MRI scheme chemistry	MASINGAR aerosol model	Yukimoto et al. (2019)
CESM2-WACCM	1º × 1º	WACCM chemistry	MAM4/MAM7 model	Danabasoglu et al. (2020)
NorESM2-LM	1.25º × 0.93º	CAM-chem set up	Oslo Aero (interactive coupled)	Seland et al. (2020)

2.2. MERRA-2 reanalysis

The MERRA-2 is developed by NASA's Global Modeling and Assimilation Office (GMAO) (Gelaro et al., 2017; Randles et al., 2017). MERRA-2 simulates several fine aerosol species such as BC, SO_4^{-2}, OC, fine dust particles and fine sea salts. It simulates aerosol species by assimilating and absorbing bias aerosol optical depth (AOD), such as those from Moderate Resolution Imaging Spectrometer (MODIS), Multiple Imaging SpectroRadiometer (MISR), Advanced Very High-Resolution Radiometer (AVHRR), ground-based Aerosol Robotic Network (AERONET) and conversional observation datasets such as those from radiosondes and aircrafts (Buchard et al., 2017). Its simulations

https://doi.org/10.5194/egusphere-2026-2738
Preprint. Discussion started: 4 June 2026

cover 72 vertical layers, from surface up to 80km using Goddard Earth Observing System, version-5 (GEOS-5) model, which is coupled to the Goddard Chemistry Aerosol Radiation and Transport (GOCART) model (Randles et al., 2017). It is advantageous in such a way that it can simulate aerosol species at fine resolution (0.5° x 0.625°) covering the entire globe with time scale of 1-hourly, 3-hourly and monthly. Its estimates have been validated and widely used to study BC different environments over the globe (Cao et al., 2021; Duc et al., 2020; Qin et al., 2019; Sarkar et al., 2019; Sitnov et al., 2020; Zhang et al., 2019).

2.3. Meteorological and other ancillary data sets

Monthly meteorological parameters such as wind, mean sea level pressure (MSLP) and atmospheric boundary layer height (BLH) from ERA5 have been used to investigate the seasonal relationship between BC and changes in meteorological parameters. ERA5 is the fifth-generation global reanalysis produced by the Copernicus Climate Change Service (C3S) under European Center for Medium-range Weather Forecast (ECMWF) (Hersbach et al., 2020). Its spatial resolution is 0.25°×0.25° covering the entire globe. The study has also utilized Climate Hazards Infrared Precipitation with station (CHIRPS) data to construct seasonal rainfall pattern over Africa. CHIRPS has been widely used and recommended for rainfall related studies over Africa (Didi et al., 2020; Dinku et al., 2018; Kouakou et al., 2023; Muthoni et al., 2019; Nkunzimana, et al., 2020). More information including data access can be found at https://climatedataguide.ucar.edu/climate-data/chirps-climate-hazards-infrared-precipitation-station-data-version-2. Burning area data between 2002 and 2020 was sourced from Global Fire Emissions (GFE) Database (https://www.globalfiredata.org/data.html) to investigate influence of changes in burning activities on the distribution of BC over Africa. The burned areas include all types of vegetation (Chen et al., 2023; Giglio et al., 2018; Hall et al., 2024), and are expressed as total burned area in each grid cell of 0.25°x0.25°.

2.4. Models evaluation and bias adjustment

AerChemMIP models simulate mass mixing ration of BC (BC_{mmr}) in the atmosphere, therefore, we converted (BC_{mmr}) into concentration (BC_{con}) by multiplying with the density of the air (Xu et al., 2022). After conversion, all model outputs and reanalysis datasets were standardized to a 0.5°×0.5° grid resolution using a bilinear interpolation method (Kim et al., 2019). MERRA-2 reanalysis was used to adjust the bias at each grid point due to lack of long-term observation that can cover the entire African continent. In addition, MERRA-2 has been proved to be consistent in capturing long-term trends and seasonality of BC against the observed data (Zhang et al., 2020; Cao et al., 2021; Mao et al., 2023; Li et al., 2024). Statistical metrics namely: Pearson's correlation (r), root mean square error (RMSE), mean bias (MB), were used for model evaluation. The general form of Pearson's correlation is expressed as;

$$r = \frac{\left[{}^{1}/_{(n-1)}\right]\sum_{i=1}^{n}[(y_{re}-\bar{y}_{re})(y_{mod}-\bar{y}_{re})]}{\left\{\left[{}^{1}/_{(n-1)}\right]\sum_{i=1}^{n}(y_{re}-\bar{y}_{re})^2\right\}^{1/2}\left\{\left[{}^{1}/_{(n-1)}\right]\sum_{i=1}^{n}(y_{mod}-\bar{y}_{mod})^2\right\}^{1/2}} \quad (1)$$

Where y_{re} and y_{mod} are the reanalysis and model simulations respectively while $\bar{y}_{re}$ and $\bar{y}_{mod}$ are their corresponding means during the period of evaluation. High positive r values imply strong positive agreement between the model and those represented in the reanalysis, whereas low or near-zero values indicate limited model skill in

https://doi.org/10.5194/egusphere-2026-2738
Preprint. Discussion started: 4 June 2026

reproducing the observed variability. Negative values indicate that the model captures variability opposite to that in the reanalysis. However, correlation only evaluates pattern agreement, not error magnitude or accuracy. Therefore, RMSE was applied to quantify the random component of the model's error, which reflects typical magnitude of model's deviations. It is highly sensitive to large errors, making it valuable for assessing model performance, mathematically expressed as;

$$\mathrm{RMSE} = \sqrt{\frac{1}{\mathrm{n}}\sum_{\mathrm{i}=1}^{\mathrm{n}}(y_{mod} - y_{re})^2} \quad (2)$$

Lower values of RMSE (~0) indicates better agreement with standard data. We also used MB to identify the systematic part of the model error, by calculating the difference between model and the reference data, expressed as;

$$\mathrm{MB} = \frac{1}{\mathrm{n}}\sum_{\mathrm{i}=1}^{\mathrm{n}}(y_{mod} - y_{re}) \quad (3)$$

Positive values of MB denote overestimation, negative values denote underestimation and values approaching zero indicate good agreement between the model and reference data with minimal systematic bias. Due to high consistence in capturing BC among the models over the domain, this study utilized index of agreement (Willmott, 1981) to select the best performing models which were used to generate a multi-model mean (MMM). Index of agreement (IA) is a standardized metric and can be used to quantify the degree of prediction error in models, offering a comprehensive assessment of model accuracy, expressed as;

$$IA = \frac{\sum_{i=1}^{n}(y_{re} - y_{mod})^2}{\sum_{i=1}^{n}(|y_{mod} - \bar{y}_{re}| + |y_{re} - \bar{y}_{re}|)^2} \quad (4)$$

IA varies between 0 and 1, where a value of 1 signifies a perfect match between model predictions and observed data, while a value of 0 indicates no agreement.

To adjust the bias in the MMM, delta change method (Sperna et al., 2010; Wu and Huang, 2016) was applied. Delta change method proved to outperforms other techniques to reduce the median absolute error between observations (reanalysis) and models (Beyer et al., 2019) despite that may not completely handle biases caused by the interaction among variables that a varying climate could intensify (Iyakaremye et al., 2021). It is expressed as;

$$y_{cor} = y_{mod} + (\bar{y}_{re} - \bar{y}_{mod}) \quad (5)$$

Lastly, a one-way analysis of variance (ANOVA), followed by post-hoc pairwise comparisons (Montgomery.2017) was applied to compare differences in mean values among the bias-adjusted MMM, unadjusted MMM and MERRA-2. This approach was used to determine whether bias adjustment significantly improved agreement with the reference dataset. Following evaluation of the bias adjustment, the bias-corrected MMM was employed in all subsequent analyses. We adopted the base period of 2004-2014 from Zanis et al. (2022) as reference period for evaluating all the AerChemMIP models.

2.5. Trends analysis

The non-parametric Sen's slope estimator (Sen, 1968) and Mann-Kendall (MK) trend test (Mann, 1945) were employed to estimate the magnitude of the trends for BC. Sen's slope provides robust estimates in the presence of

https://doi.org/10.5194/egusphere-2026-2738
Preprint. Discussion started: 4 June 2026

temporal variability and is less influenced by outliers, making it more suitable when trends are not adequately captured by parametric methods (Zarenistanak et al., 2020). MK trend test was used to understand whether BC has monotonic significant trend across the study domain. MK is advantageous in a way that it can verify the presence of trend against null hypothesis of no trend in the time series. Furthermore, it does not require the sampled data to adhere to a certain pattern as it can perform better with low or irregular values. In addition, we applied the modified MK trend test (Sneyers,1990) to detected periods of significant increase in BC concentration. The modified MK trend test is based on calculating standardized test statistic (Z-scores) derived from the original Mann Kendal trend test. For the forward sequence (starting from the first year to the last year), the Z-scores are computed incrementally by applying the MK test on increasing subsequences of the data while for backward sequence, the calculation process is the same, however, the sequence of the data is reversed. The point of intersection between the forward and backward, marks a potential shift in BC concentration levels. More details about MK computation can be accessed in other studies (Ayugi and Tan, 2019; Chatterjee et al., 2014; Oduro et al., 2022; Zarenistanak et al., 2020).

3. Results and discussion

3.1. Evaluation of AerChemMIP models

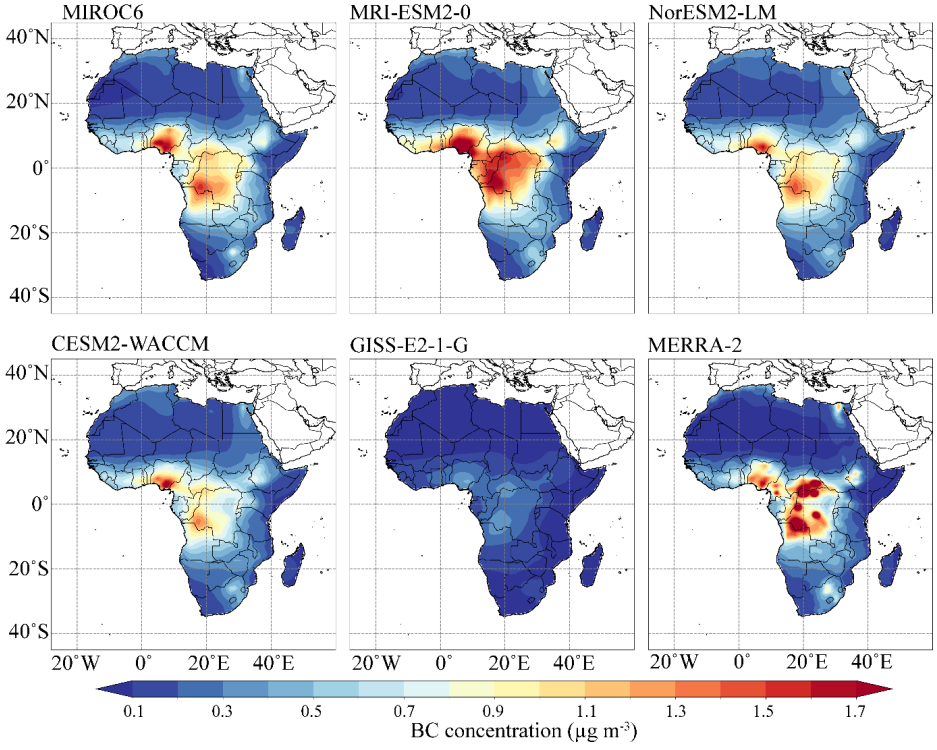

Figure 1. Spatial distribution of AerChemMIP models and MERRA-2 BC concentration during the evaluation period (2004-2014) using monthly data.

The spatial distribution of BC across all the models show high concentration in Central Africa, particularly over the Congo basin (Fig.1) while lower concentration is detected in North Africa and Madagascar Island. The observed

https://doi.org/10.5194/egusphere-2026-2738
Preprint. Discussion started: 4 June 2026

pattern is similar to the standard data (MERRA-2), implying AerChemMIP models are consistent in capturing the spatial distribution of BC in Africa. In terms of magnitude, the GISS-E2-1G exhibits the highest underestimation of compared to the rest of the models. Further analysis based on r, MB and RMSE revealed statistically significant positive correlation ($p < 0.05$) between AerChem models and MERRA-2 in most parts of the study domain (Fig.2a and Fig.3a).

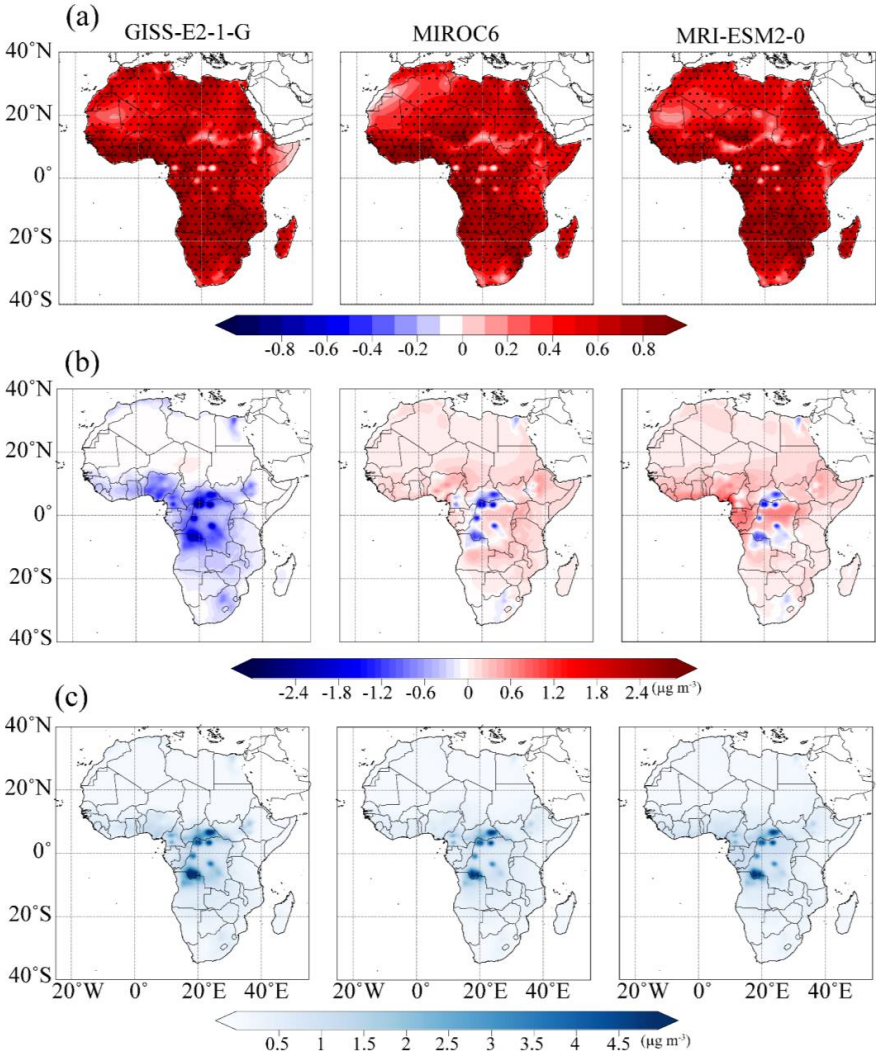

Figure 2. Spatial distribution of (a) correlation, (b) MB and (c) RMSE between AeroChemMIP models (GISS-E2-1, MIROC6 and MRI-ESM2-0) and MERRA2 during the evaluation period.

https://doi.org/10.5194/egusphere-2026-2738
Preprint. Discussion started: 4 June 2026

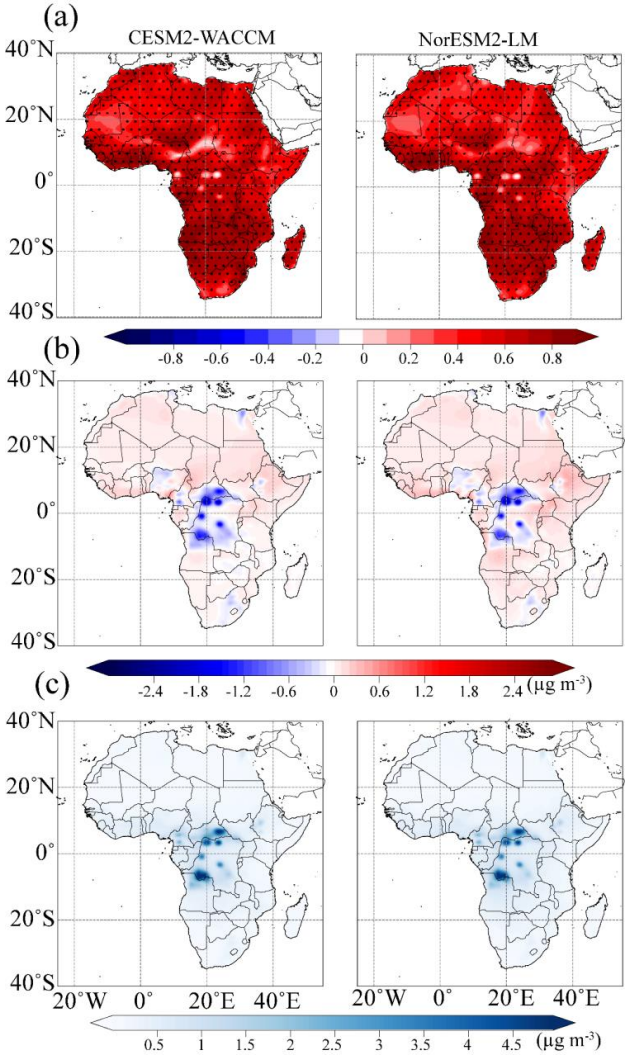

195 Figure 3. Spatial distribution of (a) correlation, (b) MB and (c) RMSE between AeroChemMIP models (CESM2-WACCM, and NorESM2-LM) and MERRA2 during the evaluation period.

However, some isolated locations in Congo and West Africa exhibit weak and non-significant correlation ($r \sim 0$, $p > 0.05$). Similar patterns are also evident between GISS-E2-1G and MERRA-2 over eastern parts of the study domain, particularly Somalia (Fig. 2). MB results (Figs.2b andFig.3b) indicate a consistent pattern among the models, with
200 regional biases ranging from approximately −2.4 to +0.6 μg m^{-3} evident over the study domain. The highest underestimation is observed in isolated parts of Central Africa for all the models. We however noted that GISS-E2-1G exhibits the largest magnitude of negative bias in most parts of Central and West Africa among the models. The observed underestimation of BC concentration by the AerChemMIP models reflects underestimation in emission inventories, particularly biomass-burning emissions, given that these regions are strongly influenced by seasonal

https://doi.org/10.5194/egusphere-2026-2738
Preprint. Discussion started: 4 June 2026

savanna fires (Keita et al., 2021). RMSE (Fig.2c and Fig.3c) further support MB results, where all the selected models revealed high values of RMSE in Central and some locations of West Africa, signifying low accuracy in capturing BC concentration over these regions. Therefore, bias correction is essential when applying AerChem models for BC-related studies over Africa.

Based on IA analysis (Fig.S2), MIROC6, MRI-ESM2-0, CESM2-WACCM and NorESM2-LM have better representation of BC concentration, with IA > 0.7 while GISS-E2-1G exhibited the lowest score (IA<0.3). IA results also agree well with results presented in Figs.2 and Fig.3, where GISS-E2-1G highly underestimated the spatial distribution of BC concentration in most places compared to other models. Consequently, MIROC6, MRI-ESM2-0, CESM2-WACCM and NorESM2-LM models were selected and used to generate MMM. It can however be noted from Fig.2, Fig.3 and Fig.S2 that the selected models still have bias against standard data. Therefore, we adjusted the bias in MMM using the method described in *section 2.2.1* and further tested its effectiveness using ANOVA. Results in (Table S1**)** demonstrated that there was no significant difference between MERRA-2 and bias adjusted MMM, implying that bias adjustment was effective, hence be used for the rest of analyses.

3.2. Annual and Seasonal dynamics of BC over Africa

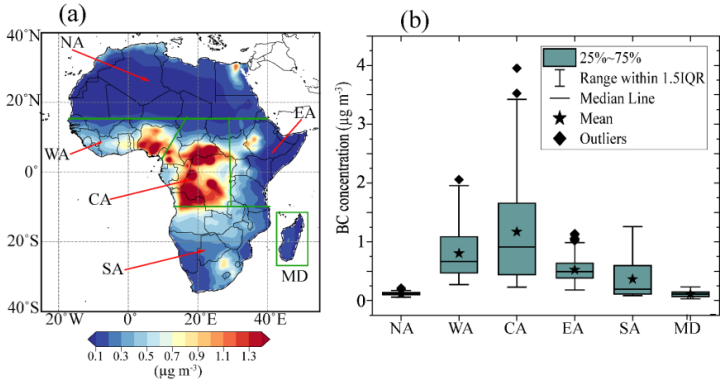

Figure 4. Spatial distribution of (a) long-term mean (1980-2023) and (b) regional average of BC concentration. Full names of the regions are: North Africa (NA), West Africa (WA), Central Africa (CA), East Africa (EA), Southern Africa (SA) and Madagascar Island (MD).

The bias-adjusted MMM (Fig.4a) revealed high annual concentration of BC in Central, followed by West Africa, specifically over Nigeria. High BC levels are also evident in northern Egypt, central parts of Ethiopia and northern parts of South Africa. Regional averages (Fig.4b) are consistent with spatial distribution, where high annual concentration of BC (>1.5μg m^{-3}) is detected in Central Africa while low (< 0.1μg m^{-3}) over North Africa and the Madagascar Island. The observed BC concentration falls within the range reported in earlier studies based on ground observations in different regions of Africa (Doumbia et al., 2012; Kuik et al., 2015; Dewitt et al., 2019; Kirago et al., 2022; Anand et al., 2024). The elevated BC concentration over Nigeria, Egypt, Ethiopia and north of South Africa is primarily driven by intensified industrial and traffic emissions (Giwa et al., 2014; Chiloane et al., 2017) while in Central Africa, seasonal biomass burning and emissions from mining zones are the dominant sources (Van Der Werf et al., 2010).

https://doi.org/10.5194/egusphere-2026-2738
Preprint. Discussion started: 4 June 2026

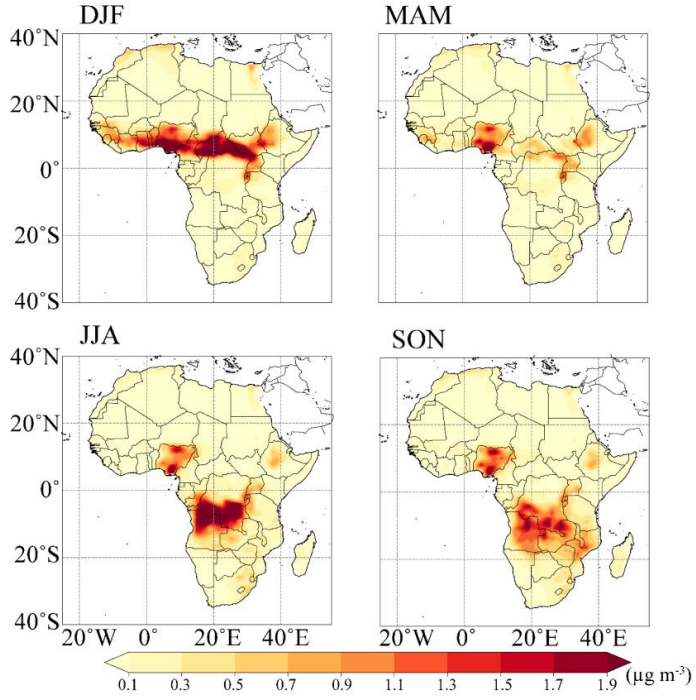

Figure 5. Seasonal spatial distribution of BC concentration over Africa for the period 1980-2014. Panels represent the four major global climatological seasons: December-February (DJF), March-May (MAM), June-August (JJA), and September-November (SON).

The seasonal spatial distribution (Fig.5) shows high BC concentration extending from East to West Africa along the 0°-15°N latitudes during DJF. During MAM, BC decrease across most regions while during JJA, BC shift southwards and peaks over Central Africa, particularly in the southern Congo and north of Angola. During SON, BC concentration shifts further south and is observed high in most parts of Southern Africa, such as in southern Congo, Zambia, Malawi, Mozambique and Zimbabwe. Increased BC concentration during SON is also notable in some locations of West Africa, specifically over Nigeria. These findings demonstrate that BC has high seasonal variation across Africa and is consistent with previous studies (Chiloane et al., 2017; Dewitt et al., 2019). Regional averages (Fig.7) also reflect the spatial patterns, with highest (> 3 μg m^{-3}) detected in Central Africa. In North Africa, a peak in BC concentration is observed during JJA and low during MAM, while West Africa exhibits peaks during DJF and minima during JJA. Central Africa shows high concentration of BC during JJA and lowest during SON while East Africa exhibits a bimodal pattern, with the first peak during DJF and a second peak during JJA. The bimodal pattern of BC observed in East Africa was also reported in Kirago et al. (2022) using ground-based observations. In Southern Africa and Madagascar Island, BC is generally highest during JJA and SON seasons respectively. The observed seasonal pattern is highly driven by the seasonal biomass burning and favorable meteorological conditions that enhance accumulation and dispersion of BC in the atmosphere (Doumbia et al., 2012; Swap et al., 2003).

https://doi.org/10.5194/egusphere-2026-2738
Preprint. Discussion started: 4 June 2026

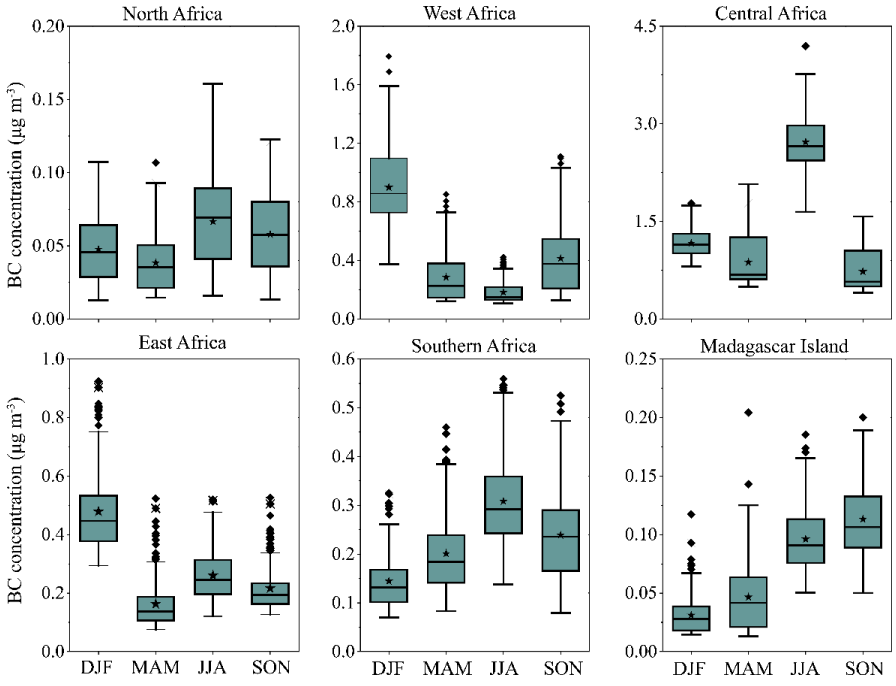

Figure 6. Box plots showing seasonal distribution of BC for each of the selected regions during 1980-2014 period.

A further comparison between seasonal distribution of BC (Fig.5) and biomass burning (Fig.S3) revealed consistence in their seasonal patterns. For instance, intense burning activities extends from East to West of Africa (along latitudes 0°-15°N) during DJF, which corresponds to high BC concentration in the same region. During MAM, burning activities decrease in most regions, leading to reduced concentration of BC in most parts while during JJA and SON, increase in burning activities correspond to increased BC levels in Central and Southern Africa respectively. Furthermore, correlation analysis between BC and total burned areas (Fig.S4) revealed statistically significant positive correlation ($p < 0.05$) in all the regions, suggesting that regional biomass burning, such as forest fires and agricultural residue burning strongly influence BC's distribution in most parts, except over North Africa where non-significant positive correlation ($r \sim 0$, $p > 0.05$) was detected. This indicates that local biomass burning in North Africa has minimal influence on BC concentration.

3.3. **Long-range transport from Europe**

Even though BC shows a weak and statistically non-significant correlation with biomass burning activities in North Africa (Fig. S4), a clear seasonal pattern is evident with concentration peaking during JJA (Fig. 6). This suggests that BC variability in the region is primarily influenced by factors other than local burning, including fossil-fuel emissions, long-range transport and meteorological conditions that favor aerosol accumulation. A previous study by Kallos et al. (1998) suggested that long-range transport from Europe may significantly influence concentration levels of pollutants in North Africa, due to its proximity to the industrialized regions and natural fires of Europe. In this study, we therefore

https://doi.org/10.5194/egusphere-2026-2738
Preprint. Discussion started: 4 June 2026

further investigated the influence from distant sources on the concentration changes of BC in North Africa using PSCF analysis (more details about PSCF are described in S1 of supplementary materials).

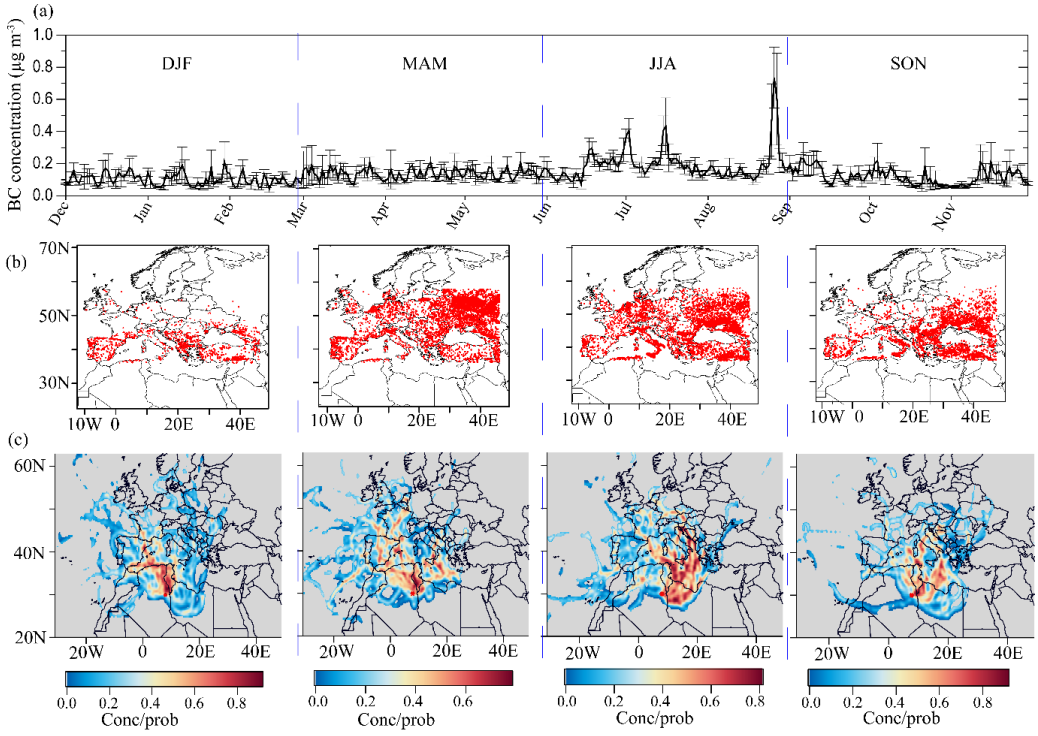

Figure 7. Daily variation of BC observed over North Africa from January to December of 2023 (a), fire hotspots from MODIS satellite (b) and PSCF to identify potential source of BC observed over North Africa (c).

We firstly correlated BC extracted over North Africa with total burned areas of Europe. Results in Fig. S5a revealed a statistically significant positive correlation ($p < 0.05$) between BC extracted over North Africa and total burned areas of Europe. Additionally, their monthly pattern (Fig.S5b) exhibited a similar variation, with peaks occurring between July and October, suggesting their strong temporal positive relationship. We then analyzed daily variation in BC concentration over a selected location in North Africa (latitude 30˚N and longitude 8˚E) and compared it with PSCF values for the year 2023. Results in Fig.7a show that BC peaks between June and August (JJA) in North Africa, which is consistent with seasonal pattern presented in Fig.6. It can also be noted that fire hotspot observations from the MODIS sensors, onboard the Terra and Aqua satellites over Europe increase from MAM to JJA, corresponding to variation of BC extracted over North Africa. Moreover, airmass trajectories tracked in North Africa during all the months (Fig. S6) originated from Europe, with some extending into North Atlantic Ocean. We also noted that airmass from Europe passed over the fire-affected regions of Europe (Fig.7b) into North Africa, which might have transported BC into North Africa. This is evident in PSCF results (Fig.7c) with high probability that portions of BC (Conc/prob) was sourced from the north, extending into Europe. High PSCF values are mostly notable over eastern Europe during DJF and MAM, while during the peak of BC (JJA), high PSCF values are observed from northeast of the tracking

https://doi.org/10.5194/egusphere-2026-2738
Preprint. Discussion started: 4 June 2026

location extending into Mediterranean Sea. The Mediterranean Sea is the major maritime route connecting Europe and Asia, hence BC emitted from maritime traffic, especially from ships, might also have been transported by the airmass into Northern Africa. This corresponds to higher PSCF values from the east of tracking point extending into Mitterrandian Sea during JJA. These results provide an evidence that long-range transport, especially those from Europe, which are mixed with maritime traffic over the Mitterrandian Sea contributes to the BC concentration levels detected over North Africa.

3.4. **Influence of regional meteorology on distribution of BC**

Apart from changes in emission sources, changes in meteorological conditions play a significant role in transportation and distribution of pollutants from the source emissions in Africa (Kallos et al.,1998; Deroubaix et al., 2019; Nyasulu et al, 2022).

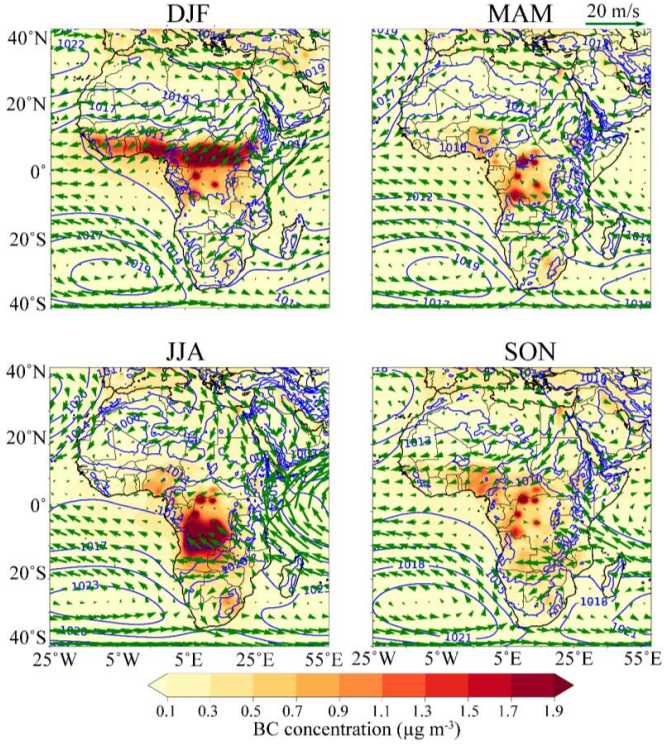

Figure 8. The composite distribution of BC, wind and mean sea level pressure (MSL) between 1980 and 2014 during different seasons over Africa. The units for MSLP are in millibars (mb).

The composite analysis of wind circulation at 850hPa, MSLP and BC (Fig.8) revealed high BC concentration associated with weak wind speed and low-pressure systems, specifically over Central Africa. Weak winds and low MSLP likely enhances accumulation of BC, leading to high concentration within Central Africa. Additionally, the

https://doi.org/10.5194/egusphere-2026-2738
Preprint. Discussion started: 4 June 2026

boundary layer height (BLH) (Fig. S7a) is consistently low throughout the seasons in Central Africa which reduces vertical dispersion, leading to accumulation of BC near the surface (Miao et al., 2018). In contrast, regions such as East and Southern Africa experience relatively stronger winds, high MSLP and increased BLH, which facilitate the dispersion of BC. It can also be noted from Fig.8 that during JJA, MSLP intensifies in the South Indian Ocean (SIO) leading to increased wind speed in most parts of Eastern and Southern Africa. This disperses BC further north to northwest, as compared to SON where pressure reduces in SIO and wind speed weakens in Southern and Eastern Africa, hence BC concentrates within the region. As similar to Southern Africa, intensified MSLP over North Africa is accompanied by strong southwesterly flow along latitudes 0˚-20˚N during DJF, which drive pollutants towards the Southwest into Atlantic Ocean (Fig.8).

Furthermore, we noted that North Africa is influenced by winds from Europe, passing over the Mediterranean Sea especially during JJA season (Fig.8). These winds likely transport BC from polluted regions of Europe and maritime traffic from Mediterranean Sea into North Africa, which corresponds to a peak in BC levels during JJA in North Africa. The observed circulation pattern complements results from potential sources based on airmass trajectories and PCSF analysis (in section 3.3: Fig.7). It is also of interest to note that BC concentration is generally high during the dry seasons along latitudes 30˚S and 40˚N, by comparing seasonal distribution in Fig.8 with seasonal rainfall pattern (Fig.S7a). This is because BC is mostly enhanced by seasonal biomass burning, which is common during the dry periods as discussed in section 3.3. Increased rainfall during wet seasons enhances wet deposition of BC in the atmosphere and dampens burning activities hence low BC. These results signify critical influence of interplay between seasonal biomass burning and metrological dynamics in driving seasonal distribution of BC across the region.

3.5. Historical trends and future projections of BC in Africa

The spatial analysis presented in Fig.S8 reveals most places in Africa experienced statistically significant positive trends of BC between 1980 and 2014. Notable hotspots of BC are Nigeria, northern Egypt, Ethiopia and Rwanda, which exhibited high-magnitude of annual trends (> 0.8% year^{-1}, $p < 0.05$). These trends are highly attributed to increased industrial activities, use of fossil-fuel and traffic emissions in these regions due to their rapid increase in economic development in the recent years (Anand et al., 2024; Chiloane et al., 2017). An exception is however observed in Central and Southwest of Africa, specifically over Namibia, where BC exhibited statistically non-significant change at annual scale ($p > 0.05$) indicating sustained levels of BC. Further regional analysis using the modified MK trend (Fig.9) aligns well with the spatial distribution patterns (Fig. S8), where most regions have experienced statistically significant positive trends in the recent years (Z-score > 1.96), except Central Africa, which exhibited a negative trend since 2008. North Africa shows a significant increase in BC concentration since early 1990s with abrupt changes detected during mid-1990s. West Africa follows a similar pattern, however, abrupt change occurred during early 2000s. East and Southern Africa also show positive trend of BC with a statistically significant change (Z-score > 1.96) since early 1990s and abrupt change in BC levels during early 2000s while Madagascar Island experienced abrupt change in BC levels during mid-1990s. These abrupt trend shifts indicate critical turning points in BC concentration levels across Africa, which coincides with rising industrial activities, increased traffic emissions and changes in biomass burning practices (Keita et al., 2021). The statistically significant increase in BC (Z-score >

https://doi.org/10.5194/egusphere-2026-2738
Preprint. Discussion started: 4 June 2026

1.96) , observed in most regions pose substantial risks to both climate and public health, hence regionally tailored policies to reduce BC levels in the atmosphere are essential across Africa.

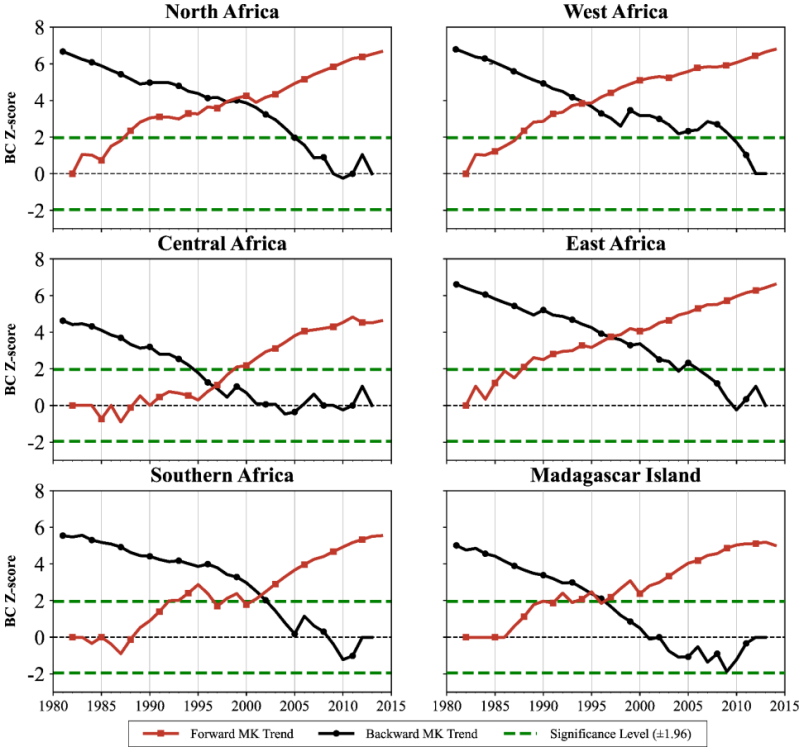

Figure 9. Temporal distribution of BC trends during 1981-2014 period using the modified MK trend test.

The projected trends under the SSP370SST (Fig.10) show that during the near-term (2015-2040), BC trends are predominantly positive across North and West Africa, with an increase exceeding ~0.5-1.0% yr^{-1}, indicating intensified BC during the near-term. In contrast, Central and Southern Africa exhibit weak to moderate negative trends, suggesting localized emission reductions. By mid-century (2041-2070), positive trends persist and strengthen over West Africa and parts of North Africa, indicating these regions are future hotspots of BC hence require enhanced intervention. Southern Africa shows stronger negative trends, reflecting mitigation progress. Central, East Africa and Madagascar Island project mixed patterns during mid-century, indicating emerging regions of concern where emissions may increase without targeted policies. In the late-century period (2071-2100), a marked shift occurs, with North Africa transitioning to negative trends and widespread declines across Central and Southern Africa, suggesting improved emission controls, however, localized positive trends in East Africa and Madagascar Island indicate that the region becomes a priority for late-century mitigation efforts.

These projected trends have important implications for human health, climate forcing and targeted mitigation strategies. The strong increase in BC over North and West Africa during near and mid-century implies high health risks and enhanced atmospheric heating, which can intensify regional warming and disrupt precipitation patterns and accelerate extreme weather events (Bobde et al., 2025; Nnamchi and Fiedler, 2026), underscoring the need for early

https://doi.org/10.5194/egusphere-2026-2738
Preprint. Discussion started: 4 June 2026

and aggressive emission controls in these regions, particularly with focus on transport, residential energy and industrial emissions. The persistence of elevated BC in West Africa into the mid-century indicates that the region needs most sustained intervention across multiple decades. Conversely, the decline in BC over Southern Africa, especially after mid-century, suggests that existing or evolving mitigation measures may be effective and should be sustained. These results emphasize that mitigation priorities in Africa shift across regions and time, requiring a dynamic and region-specific approach. Immediate action is needed in North and West Africa, alongside sustained intervention in West Africa and continued monitoring in East Africa. Meanwhile, mitigation efforts should be maintained in parts of Central and Southern Africa to keep BC at lower levels throughout the century.

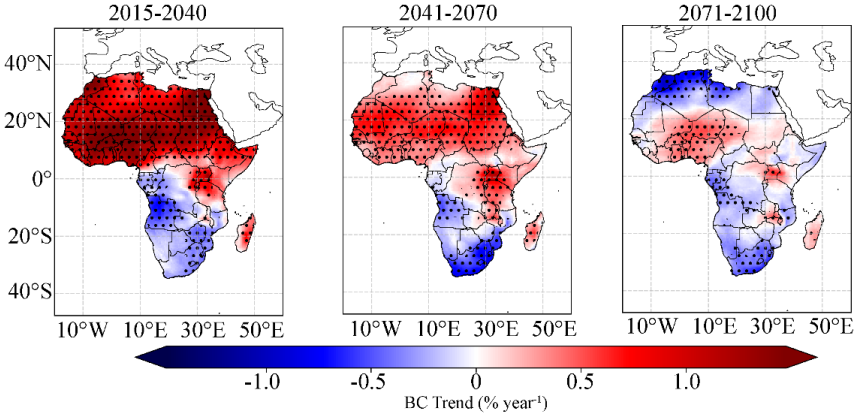

Figure 10. Projected changes of BC trends (by percentage) over Africa. 2015-2040 represents near future, 2041-2070 represents middle of the Century while 2071-2100 represents future period.

4. Conclusions

This study has used bias adjusted AerChemMIP-CMIP6 models to investigated the hotspot regions of BC and the driving factors across Africa. Findings show that the models effectively captured the spatial distribution of BC across Africa, although regional biases ranging from approximately -2.4 to +0.6 μg m^{-3} were evident. The largest underestimations (up to ~2.4 μg m^{-3}) occurred in isolated locations of Central Africa. Therefore, bias adjustment is essential when applying AerChemMIP models in BC-related studies over the continent. Based on bias adjusted model mean, elevated concentration of BC (> 1.5 μg m^{-3}) is recorded in Central Africa, while low (< 0.1 μg m^{-3}) in most parts of North Africa and Madagascar Island. The seasonal distribution exhibits peaks during the dry seasons in most regions, strongly driven by seasonal biomass burning and prevailing meteorological conditions while long-range transport from Europe influences BC concentration in North Africa. Trend analyses reveal a statistically significant increasing in BC levels, with the highest detected in industrialized and densely populated regions, such as Southern Nigeria, Central Ethiopia and Northern Egypt, with the annual growth rate surpasses 1 % yr^{-1}.

https://doi.org/10.5194/egusphere-2026-2738
Preprint. Discussion started: 4 June 2026

These findings have demonstrated that without targeted intervention, BC concentration is likely to increase across North, West, East Africa and Madagascar through the mid-21st century, driven primarily by growing fossil fuel use, traffic emissions and reliance on biomass for household energy. This projected rise suggests a worsening of air quality and contribution to regional warming, potentially offsetting climate mitigation gains. In contrast, the declining trends projected over Southern and parts of Central Africa indicate that emission reductions are achievable and may already reflect effective policies or lower emission intensities. This study hence strongly recommends targeted control measures and stricter policies to reduce industrial and traffic emissions in regions with rapid economic growth and fossil fuel emissions such as in West, North and East Africa. Findings from this study provide critical guidance for policy interventions of mitigating BC concentration in the atmosphere across the African continent.

Data availability

Coupled Model Intercomparison Project Phase 6 (CMIP6) data; https://esgf-node.ipsl.upmc.fr/projects/cmip6-ipsl/. Modern-Era Retrospective Analysis for Research and Applications Version 2 (MERRA-2) reanalysis: https://disc.gsfc.nasa.gov/. European Centre for Medium-range Weather Forecast (ECMWF) reanalysis: https://cds.climate.copernicus.eu/datasets.

Global Data Assimilation System (GDAS) meteorological data: https://www.ready.noaa.gov/data/archives/gdas1/. The Moderate Resolution Imaging Spectroradiometer (MODIS) fire data: https://firms.modaps.eosdis.nasa.gov/download/.

Authors contribution

MN; Data analysis and writing the original draft, YLZ; Conceptualization and supervision, CF: Editing and reviewing, Md MH: editing.

Competing of interest

The authors declare no competing interests.

Acknowledgements

The authors acknowledge funding from the National Natural Science Foundation of China (Grant 42325304).

References

Ali, M. U., Siyi, L., Yousaf, B., Abbas, Q., Hameed, R., Zheng, C., … Wong, M. H.: Emission sources and full spectrum of health impacts of black carbon associated polycyclic aromatic hydrocarbons (PAHs) in urban environment: A review, Critical Reviews in Environmental Science and Technology, 51(9), 857–896. https://doi.org/10.1080/10643389.2020.1738854, 2021.

Allen, R. J., Turnock, S., Nabat, P., Neubauer, D., Lohmann, U., Olivié, D., … Tsigaridis, K.: Climate and air quality impacts due to mitigation of non-methane near-term climate forcers, Atmospheric Chemistry and Phys, (December 2019), 9641–9663, 2020.

Alli, A. S., Clark, S. N., Hughes, A., Nimo, J., Bedford-Moses, J., Baah, S., … Arku, R. E.: Spatial-temporal patterns of ambient fine particulate matter (PM2.5) and black carbon (BC) pollution in Accra, Environmental Research

https://doi.org/10.5194/egusphere-2026-2738
Preprint. Discussion started: 4 June 2026

Letters, 16(7). https://doi.org/10.1088/1748-9326/ac074a, 2021.

Anand, A., Touré, N. E., Bahino, J., Gnamien, S., Hughes, A. F., Arku, R. E., … Presto, A. A.: Low-Cost Hourly Ambient Black Carbon Measurements at Multiple Cities in Africa, Environmental Science and Technology, 58(28), 12575–12584. https://doi.org/10.1021/acs.est.4c02297, 2024

Ayugi, B. O., and Tan, G.: Recent trends of surface air temperatures over Kenya from 1971 to 2010, Meteorology and Atmospheric Physics, 131(5), 1401–1413. https://doi.org/10.1007/s00703-018-0644-z, 2019

Beyer, R., Krapp, M., and Manica, A.: A systematic comparison of bias correction methods for paleoclimate simulations, A Systematic Comparison of Bias Correction Methods for Paleoclimate Simulations, (February), 1–23, 2019

Bobde, V., Ayegbusi, K., Akinsanola, A. A., Morakinyo, T. E., and Adebiyi, A. A.: Anthropogenic warming is accelerating recent heatwaves in Africa, Communications Earth and Environment, 1–12. Retrieved from https://doi.org/10.1038/s43247-025-02578-6,2025.

Bond, T. C., Doherty, S. J., Fahey, D. W., Forster, P. M., Berntsen, T., Deangelo, B. J., … Quinn, P. K.: Bounding the role of black carbon in the climate system : A scienti fi c assessment. Journal of Geophysical Research: Atmosphere, 118, 5380–5552. https://doi.org/10.1002/jgrd.50171,2013.

Boucher, O., and Haywood, J.: On summing the components of radiative forcing of climate change, Climate Dynamics, 18(3–4), 297–302. https://doi.org/10.1007/s003820100185, 2001.

Buchard, V., Randles, C. A., da Silva, A. M., Darmenov, A., Colarco, P. R., Govindaraju, R., … Yu, H.: The MERRA-2 aerosol reanalysis, 1980 onward. Part II: Evaluation and case studies, Journal of Climate, 30(17), 6851–6872. https://doi.org/10.1175/JCLI-D-16-0613.1, 2017.

Cao, S., Zhang, S., Gao, C., Yan, Y., Bao, J., Su, L., … Liu, M.: A long-term analysis of atmospheric black carbon MERRA-2 concentration over China during 1980–2019, Atmospheric Environment, 264(July), 118662. https://doi.org/10.1016/j.atmosenv.2021.118662, 2021.

Cape, J. N., Coyle, M., and Dumitrean, P.: The atmospheric lifetime of black carbon, Atmospheric Environment, 59, 256–263. https://doi.org/10.1016/j.atmosenv.2012.05.030, 2012.

Chatterjee, S., Bisai, D., and Khan, A. (2014). Detection of Approximate Potential Trend Turning Points in Temperature Time Series (1941-2010) for Asansol Weather Observation Station, West Bengal, India, Atmospheric and Climate Sciences, 04(01), 64–69. https://doi.org/10.4236/acs.2014.41009, 2014.

Chen, Y., Hall, J., Van Wees, D., Andela, N., Hantson, S., Giglio, L., … Randerson, J. T.: Multi-decadal trends and variability in burned area from the fifth version of the Global Fire Emissions Database (GFED5). Earth System Science Data, 15(11), 5227–5259. https://doi.org/10.5194/essd-15-5227-2023, 2023.

Chiloane, K. E., Beukes, J. P., Van Zyl, P. G., Maritz, P., Vakkari, V., Josipovic, M., … Laakso, L.: Spatial, temporal and source contribution assessments of black carbon over the northern interior of South Africa, Atmospheric Chemistry and Physics, 17(10), 6177–6196. https://doi.org/10.5194/acp-17-6177-2017, 2017.

Collins, J. W., Lamarque, J. F., Schulz, M., Boucher, O., Eyring, V., Hegglin, I. M., … Smith, J. S.: AerChemMIP: Quantifying the effects of chemistry and aerosols in CMIP6, Geoscientific Model Development, 10(2), 585–607. https://doi.org/10.5194/gmd-10-585-2017, 2017.

https://doi.org/10.5194/egusphere-2026-2738
Preprint. Discussion started: 4 June 2026

Danabasoglu, G., Lamarque, J. F., Bacmeister, J., Bailey, D. A., DuVivier, A. K., Edwards, J., … Strand, W. G.: The Community Earth System Model Version 2 (CESM2), Journal of Advances in Modeling Earth Systems, 12(2), 1–35. https://doi.org/10.1029/2019MS001916, 2020.

Dawoud, W., El Kenawy, A. M., Abdel Wahab, M. M., and Oraby, A. H.: Temporal Variability of Particulate Matter and Black Carbon Concentrations over Greater Cairo and Its Atmospheric Drivers, Climate, 11(7). https://doi.org/10.3390/cli11070133, 2023.

Didi Sacré Regis, M., Mouhamed, L., Kouakou, K., Adeline, B., Arona, D., Saint, C. H. J., … Issiaka, S.: Using the CHIRPS dataset to investigate historical changes in precipitation extremes in West Africa, Climate, 8(7). https://doi.org/10.3390/CLI8070084, 2020.

Dinku, T., Funk, C., Peterson, P., Maidment, R., Tadesse, T., Gadain, H., and Ceccato, P.: Validation of the CHIRPS satellite rainfall estimates over eastern Africa, Quarterly Journal of the Royal Meteorological Society, 144(June 2017), 292–312. https://doi.org/10.1002/qj.3244, 2018.

Doumbia, E. H. T., Liousse, C., Galy-Lacaux, C., Ndiaye, S. A., Diop, B., Ouafo, M., … Sigha, L.: Real time black carbon measurements in West and Central Africa urban sites, Atmospheric Environment, 54, 529–537. https://doi.org/10.1016/j.atmosenv.2012.02.005, 2012.

Duc, H. N., Shingles, K., White, S., Salter, D., Chang, L. T. C., Gunashanhar, G., … Kirkwood, J. (2020). Spatial-temporal pattern of black carbon (BC) emission from biomass burning and anthropogenic sources in New South Wales and the greater metropolitan region of Sydney, Australia, Atmosphere, 11(6). https://doi.org/10.3390/atmos11060570

Gelaro, R., McCarty, W., Suárez, M. J., Todling, R., Molod, A., Takacs, L., … Zhao, B.: The modern-era retrospective analysis for research and applications, version 2 (MERRA-2). Journal of Climate, 30(14), 5419–5454. https://doi.org/10.1175/JCLI-D-16-0758.1, 2017.

Ghosh, S., Verma, S., Kuttippurath, J., and Menut, L.: Wintertime direct radiative effects due to black carbon (BC) over the Indo-Gangetic Plain as modelled with new BC emission inventories in CHIMERE, Atmospheric Chemistry and Physics, 21(10), 7671–7694. https://doi.org/10.5194/acp-21-7671-2021, 2021.

Giglio, L., Boschetti, L., Roy, D. P., Humber, M. L., and Justice, C. O.: The Collection 6 MODIS burned area mapping algorithm and product, Remote Sensing of Environment, 217(August), 72–85. https://doi.org/10.1016/j.rse.2018.08.005, 2018.

Giwa, S. O., Adama, O. O., and Akinyemi, O. O.: Baseline black carbon emissions for gas flaring in the Niger Delta region of Nigeria, Journal of Natural Gas Science and Engineering, 20, 373–379. https://doi.org/10.1016/j.jngse.2014.07.026, 2014.

Griffiths, P. T., Wilcox, L. J., Allen, R. J., Naik, V., O'Connor, F. M., Prather, M., … Young, P. J.: Opinion: The role of AerChemMIP in advancing climate and air quality research, Atmospheric Chemistry and Physics, 25(14), 8289–8328. https://doi.org/10.5194/acp-25-8289-2025, 2025.

Hersbach, H., Bell, B., Berrisford, P., Hirahara, S., Horányi, A., Muñoz-Sabater, J., … Thépaut, J. N.: The ERA5 global reanalysis, Quarterly Journal of the Royal Meteorological Society, 146(730), 1999–2049. https://doi.org/10.1002/qj.3803, 2020.

https://doi.org/10.5194/egusphere-2026-2738
Preprint. Discussion started: 4 June 2026

Hoesly, R. M., Smith, S. J., Feng, L., Klimont, Z., Janssens-Maenhout, G., Pitkanen, T., … Zhang, Q.: Historical (1750--2014) anthropogenic emissions of reactive gases and aerosols from the Community Emissions Data System (CEDS), Geoscientific Model Development, 11(1), 369–408. https://doi.org/10.5194/gmd-11-369-2018, 2018.

Hsu, N. C., Jeong, M., Bettenhausen, C., Sayer, A. M., Hansell, R., Seftor, C. S., … Tsay, S.: Enhanced Deep Blue aerosol retrieval algorithm : The second generation, Journal of Geophysical Research: Atmosphere, 118, 1–20. https://doi.org/10.1002/jgrd.50712, 2013.

Iyakaremye, V., Zeng, G., Yang, X., Zhang, G., Ullah, I., Gahigi, A., … Ayugi, B.: Increased high-temperature extremes and associated population exposure in Africa by the mid-21st century, Science of the Total Environment, 790, 148162. https://doi.org/10.1016/j.scitotenv.2021.148162, 2021.

Jacobson, M. Z.: Strong radiative heating due to the mixing state of black carbon in atmospheric aerosols, Nature, 409(6821), 695–697. https://doi.org/10.1038/35055518, 2001.

Janssen, N. A. H., Hoek, G., Simic-Lawson, M., Fischer, P., van Bree, L., Brink, H. Ten, … Cassee, F. R.: Black carbon as an additional indicator of the adverse health effects of airborne particles compared with pm10 and pm2.5, Environmental Health Perspectives, 119(12), 1691–1699. https://doi.org/10.1289/ehp.1003369, 2011.

Kallos, G., Kotroni, V., Lagouvardos, K., and Papadopoulos, A.: On the long-range transport of air pollutants from Europe to Africa, Geophysical Research Letters, 25(5), 619–622. https://doi.org/10.1029/97GL03317, 1998.

Keita, S., Liousse, C., Assamoi, E. M., Doumbia, T., N'Datchoh, E. T., Gnamien, S., … Yoboué, V.: African anthropogenic emissions inventory for gases and particles from 1990 to 2015, Earth System Science Data, 13(7), 3691–3705. https://doi.org/10.5194/essd-13-3691-2021, 2021.

Kelley, M., Schmidt, G. A., Nazarenko, L. S., Bauer, S. E., Ruedy, R., Russell, G. L., … Yao, M. S.: GISS-E2.1: Configurations and Climatology, Journal of Advances in Modeling Earth Systems, 12(8), 1–38. https://doi.org/10.1029/2019MS002025, 2020.

Kim, K. H., Shim, P. S., and Shin, S.: An alternative bilinear interpolation method between spherical grids, Atmosphere, 10(3). https://doi.org/10.3390/atmos10030123, 2019.

Kirago, L., Gatari, M. J., Gustafsson, Ö., and Andersson, A.: Black carbon emissions from traffic contribute substantially to air pollution in Nairobi, Kenya, Communications Earth and Environment, 3(1), 1–8. https://doi.org/10.1038/s43247-022-00400-1, 2022.

Kirago, L., Gustafsson, Ö., Gaita, S. M., Haslett, S. L., Dewitt, H. L., Gasore, J., … Andersson, A.: Atmospheric Black Carbon Loadings and Sources over Eastern Sub-Saharan Africa Are Governed by the Regional Savanna Fires, Environmental Science and Technology, 56(22), 15460–15469. https://doi.org/10.1021/acs.est.2c05837, 2022.

Kirchstetter, T. W., Novakov, T., Hobbs, P. V., and Magi, B.: Airborne measurements of carbonaceous aerosols in southern Africa during the dry biomass burning season, Journal of Geophysical Research: Atmospheres, 108(13). https://doi.org/10.1029/2002jd002171, 2003.

Kouakou, C., Paturel, J. E., Satgé, F., Tramblay, Y., Defrance, D., and Rouché, N.: Comparison of gridded precipitation estimates for regional hydrological modeling in West and Central Africa, Journal of Hydrology:

https://doi.org/10.5194/egusphere-2026-2738
Preprint. Discussion started: 4 June 2026

Regional Studies, 47(April), 1–23. https://doi.org/10.1016/j.ejrh.2023.101409, 2023.

Langley Dewitt, H., Gasore, J., Rupakheti, M., Potter, K. E., Prinn, R. G., De Dieu Ndikubwimana, J., … Safari, B.: Seasonal and diurnal variability in O3, black carbon, and CO measured at the Rwanda Climate Observatory, Atmospheric Chemistry and Physics, 19(3), 2063–2078. https://doi.org/10.5194/acp-19-2063-2019, 2019.

Mann, H. B.: Nonparametric Tests Against Trend, Econometrica, 13(3), 245–259. https://doi.org/10.2307/1907187, 1945.

Miao, Y., Liu, S., Guo, J., Huang, S., Yan, Y., and Lou, M.: Unraveling the relationships between boundary layer height and PM2.5 pollution in China based on four-year radiosonde measurements, Environmental Pollution, 243, 1186–1195. https://doi.org/10.1016/j.envpol.2018.09.070, 2018.

Muthoni, F. K., Odongo, V. O., Ochieng, J., Mugalavai, E. M., Mourice, S. K., Hoesche-Zeledon, I., … Bekunda, M.: Long-term spatial-temporal trends and variability of rainfall over Eastern and Southern Africa. Theoretical Appllied Climatology, 137(3–4), 1869–1882. https://doi.org/10.1007/s00704-018-2712-1, 2019.

Nkunzimana, A., Bi, S., Alriah, M. A. A., Zhi, T., and Kur, N. A. D.: Comparative Analysis of the Performance of Satellite-Based Rainfall Products Over Various Topographical Unities in Central East Africa: Case of Burundi. Earth and Space Science, 7(5). https://doi.org/10.1029/2019EA000834, 2020.

Nnamchi, H. C., and Fiedler, S.: Anthropogenic aerosols override greenhouse gases in Sahel climate change. Communications Earth and Environment, 7(1), 331. https://doi.org/10.1038/s43247-026-03474-3, 2026.

Nyasulu, M., Haque, M. M., Musonda, B., and Fang, C.: The long-term spatial and temporal distribution of aerosol optical depth and its associated atmospheric circulation over Southeast Africa. Environtal Science and Pollution Research, (0123456789). https://doi.org/10.1007/s11356-021-18446-7, 2022.

O'Neill, B. C., Kriegler, E., Ebi, K. L., Kemp-Benedict, E., Riahi, K., Rothman, D. S., … Solecki, W.: The roads ahead: Narratives for shared socioeconomic pathways describing world futures in the 21st century, Global Environmental Change, 42, 169–180. https://doi.org/10.1016/j.gloenvcha.2015.01.004, 2017.

Oduro, C., Shuoben, B., Ayugi, B., Beibei, L., Babaousmail, H., Sarfo, I., … Ngoma, H.: Observed and Coupled Model Intercomparison Project 6 multimodel simulated changes in near-surface temperature properties over Ghana during the 20th century, International Journal of Climatology, 42(7), 3681–3701. https://doi.org/10.1002/joc.7439, 2022.

Oluleye, A., and Folorunsho, A.: Black carbon pollution simulations: a RegCM4 model projection and assessment during the boreal winter and summer over West Africa region, Modeling Earth Systems and Environment, 7(4), 2313–2327. https://doi.org/10.1007/s40808-020-00976-7, 2021.

Qin, W., Zhang, Y., Chen, J., Yu, Q., Cheng, S., Li, W., … Tian, H.: Variation, sources and historical trend of black carbon in Beijing, China based on ground observation and MERRA-2 reanalysis data, Environmental Pollution, 245(2), 853–863. https://doi.org/10.1016/j.envpol.2018.11.063, 2019.

Ramanathan, V., and Carmichael, G.: Global and regional climate changes due to black carbon, Nature Geoscience, 1(4), 221–227. https://doi.org/10.1038/ngeo156, 2008.

Randles, C. A., da Silva, A. M., Darmenov, A., Govindaraju, R., Smirnov, A., Hair, J., … Flynn, C. J.: The MERRA-2 Aerosol Reanalysis , 1980 Onward . Part I : System Description and Data Assimilation Evaluation. Journal of

https://doi.org/10.5194/egusphere-2026-2738
Preprint. Discussion started: 4 June 2026

Climate., 6823–6850. https://doi.org/10.1175/JCLI-D-16-0609.1, 2017.

Rawat, P., Sarkar, S., Jia, S., Khillare, P. S., and Sharma, B.: Regional sulfate drives long-term rise in AOD over megacity Kolkata, India, Atmospheric Environment, 209(111), 167–181. https://doi.org/10.1016/j.atmosenv.2019.04.031, 2019.

Samset, B. H., Myhre, G., Herber, A., Kondo, Y., Li, S. M., Moteki, N., … Zhang, K.: Modelled black carbon radiative forcing and atmospheric lifetime in AeroCom Phase II constrained by aircraft observations, Atmospheric Chemistry and Physics, 14(22), 12465–12477. https://doi.org/10.5194/acp-14-12465-2014, 2014.

Segersson, D., Eneroth, K., Gidhagen, L., Johansson, C., Omstedt, G., Nylén, A. E., and Forsberg, B.: Health impact of PM10, PM2.5 and black carbon exposure due to different source sectors in Stockholm, Gothenburg and Umea, Sweden, International Journal of Environmental Research and Public Health, 14(7), 11–14. https://doi.org/10.3390/ijerph14070742, 2017.

Seland, Ø., Bentsen, M., Olivié, D., Toniazzo, T., Gjermundsen, A., Graff, L. S., … Schulz, M.: Overview of the Norwegian Earth System Model (NorESM2) and key climate response of CMIP6 DECK, historical, and scenario simulations, Geoscientific Model Development (Vol. 13). https://doi.org/10.5194/gmd-13-6165-2020, 2020.

Sen, P. K.: Estimates of the Regression Coefficient Based on Kendall's Tau. Journal of the American Statistical Association, 63(324), 1379–1389. https://doi.org/10.1080/01621459.1968.10480934, 1968.

Shiogama, H., Tatebe, H., Hayashi, M., Abe, M., Arai, M., Koyama, H., … Watanabe, M.: MIROC6 Large Ensemble (MIROC6-LE): experimental design and initial analyses, Earth System Dynamics, 14(6), 1107–1124. https://doi.org/10.5194/esd-14-1107-2023, 2023.

Sitnov, S. A., Mokhov, I. I., and Likhosherstova, A. A.: Exploring large-scale black‐carbon air pollution over Northern Eurasia in summer 2016 using MERRA-2 reanalysis data, Atmospheric Research, 235(November 2019), 104763. https://doi.org/10.1016/j.atmosres.2019.104763, 2020.

Sperna Weiland, F. C., Van Beek, L. P. H., Kwadijk, J. C. J., and Bierkens, M. F. P.: The ability of a GCM-forced hydrological model to reproduce global discharge variability, Hydrology and Earth System Sciences, 14(8), 1595–1621. https://doi.org/10.5194/hess-14-1595-2010, 2010.

Swap, R. J., Annegarn, H. J., Suttles, J. T., King, M. D., Platnick, S., Privette, J. L., and Scholes, R. J.: Africa burning : A thematic analysis of the Southern African Regional Science Initiative (SAFARI 2000), 108(Safari 2000), Journal of Geophysical Research: Atmosphere, 1–15. https://doi.org/10.1029/2003JD003747, 2003.

Thornhill, G. D., Collins, W. J., Kramer, R. J., Olivié, D., Skeie, R. B., O'Connor, F. M., … Zhang, J.: Effective radiative forcing from emissions of reactive gases and aerosols -- a multi-model comparison, Atmospheric Chemistry and Physics, 21(2), 853–874. https://doi.org/10.5194/acp-21-853-2021, 2021.

Toolan, C. A., Amooli, J. A., Wilcox, L. J., Samset, B. H., Turner, A. G., & Westervelt, D. M.: Strong intermodel differences and biases in CMIP6 simulations of PM$_{2.5}$, aerosol optical depth, and precipitation over Africa, Atmospheric Chemistry and Physics, 25(18), 10523–10557. https://doi.org/10.5194/acp-25-10523-2025, 2025.

Turnock, S. T., Allen, R. J., Andrews, M., Bauer, S. E., Deushi, M., Emmons, L., … Zhang, J.: Historical and future changes in air pollutants from CMIP6 models, Atmospheric Chemistry and Physics, 20(23), 14547–14579.

https://doi.org/10.5194/egusphere-2026-2738
Preprint. Discussion started: 4 June 2026

https://doi.org/10.5194/acp-20-14547-2020, 2020.

Van Der Werf, G. R., Randerson, J. T., Giglio, L., Collatz, G. J., Mu, M., Kasibhatla, P. S., … Van Leeuwen, T. T.: . Global fire emissions and the contribution of deforestation, savanna, forest, agricultural, and peat fires (1997-2009). Atmospheric Chemistry and Physics, 10(23), 11707–11735. https://doi.org/10.5194/acp-10-11707-2010, 2010.

Willmott, C. J.: ON THE VALIDATION OF MODELS. Physical Geography, 2(2), 184–194. https://doi.org/10.1080/02723646.1981.10642213, 1981.

Wu, C., and Huang, G.: Projection of climate extremes in the Zhujiang River basin using a regional climate model, International Journal of Climatology, 36(3), 1184–1196. https://doi.org/10.1002/joc.4412, 2016.

Xu, Y., Wu, J., and Han, Z.: Evaluation and Projection of Surface PM2.5 and Its Exposure on Population in Asia Based on the CMIP6 GCMs, International Journal of Environmental Research and Public Health, 19(19). https://doi.org/10.3390/ijerph191912092, 2022.

Yukimoto, S., Kawai, H., Koshiro, T., Oshima, N., Yoshida, K., Urakawa, S., … Ishii, M.: The meteorological research institute Earth system model version 2.0, MRI-ESM2.0: Description and basic evaluation of the physical component, Journal of the Meteorological Society of Japan, 97(5), 931–965. https://doi.org/10.2151/jmsj.2019-051, 2019.

Zanis, P., Akritidis, D., Turnock, S., Naik, V., Szopa, S., Georgoulias, A. K., … Van Noije, T.: Climate change penalty and benefit on surface ozone: A global perspective based on CMIP6 earth system models, Environmental Research Letters, 17(2). https://doi.org/10.1088/1748-9326/ac4a34, 2022.

Zarenistanak, M., Dhorge, A. G., and Kripalani, R. H.: Trend analysis and change point detection of seasonal and annual precipitation in Iran, International Journal of Climatology., 40(1), 308–323. https://doi.org/10.1002/joc.6211, 2020.

Zhang, Y., Jin, J., Li, Y., Yu, D., Zhou, Q., and Gao, L.: Characteristics of MERRA-2 Black Carbon in Eight Key Climatic Regions across China from 2007 to 2018, E3S Web of Conferences, 194, 1–5. https://doi.org/10.1051/e3sconf/202019404060, 2020.

Zhang, Y., Li, Y., Guo, J., Wang, Y., Chen, D., and Chen, H.: The climatology and trend of black carbon in China from 12-year ground observations, Climate Dynamics, 53(9–10), 5881–5892. https://doi.org/10.1007/s00382-019-04903-0, 2019.